Atmos. Chem. Phys., 11, 9253–9269, 2011
www.atmos-chem-phys.net/11/9253/2011/
doi:10.5194/acp-11-9253-2011

Atmospheric Chemistry and Physics

Carbon monoxide (CO) and ethane (C_2H_6) trends from ground-based solar FTIR measurements at six European stations, comparison and sensitivity analysis with the EMEP model

J. Angelbratt[1], J. Mellqvist[1], D. Simpson[1,3], J. E. Jonson[3], T. Blumenstock[7], T. Borsdorff[6], P. Duchatelet[4], F. Forster[6], F. Hase[7], E. Mahieu[4], M. De Mazière[2], J. Notholt[5], A. K. Petersen[5,*], U. Raffalski[7], C. Servais[4], R. Sussmann[6], T. Warneke[5], and C. Vigouroux[2]

[1]Chalmers University of Technology, Göteborg, Sweden
[2]Belgian Institute for Space Aeronomy (BIRA-IASB), Brussels, Belgium
[3]EMEP MSC-W, Norwegian Meteorological Institute, Oslo, Norway
[4]Institute of Astrophysics and Geophysics, University of Liège, Liège, Belgium
[5]Institute of Environmental Physics, University of Bremen, Bremen, Germany
[6]Karlsruhe Institute of Technology (KIT), Institute for Meteorology and Climate Research (IMK-ASF), Garmisch-Patenkirchen, Germany
[7]Karlsruhe Institute of Technology (KIT), Institute for Meteorology and Climate Research (IMK-ASF), Karlsruhe, Germany
[*]Present address: Max-Planck-Institute for Meteorology, Hamburg, Germany

Received: 22 March 2011 – Published in Atmos. Chem. Phys. Discuss.: May 2011
Revised: 9 August 2011 – Accepted: 28 August 2011 – Published: 8 September 2011

Abstract. Trends in the CO and C_2H_6 partial columns (∼0–15 km) have been estimated from four European ground-based solar FTIR (Fourier Transform InfraRed) stations for the 1996–2006 time period. The CO trends from the four stations Jungfraujoch, Zugspitze, Harestua and Kiruna have been estimated to $-0.45 \pm 0.16\,\%\,yr^{-1}$, $-1.00 \pm 0.24\,\%\,yr^{-1}$, $-0.62 \pm 0.19\,\%\,yr^{-1}$ and $-0.61 \pm 0.16\,\%\,yr^{-1}$, respectively. The corresponding trends for C_2H_6 are $-1.51 \pm 0.23\,\%\,yr^{-1}$, $-2.11 \pm 0.30\,\%\,yr^{-1}$, $-1.09 \pm 0.25\,\%\,yr^{-1}$ and $-1.14 \pm 0.18\,\%\,yr^{-1}$. All trends are presented with their 2-σ confidence intervals. To find possible reasons for the CO trends, the global-scale EMEP MSC-W chemical transport model has been used in a series of sensitivity scenarios. It is shown that the trends are consistent with the combination of a 20 % decrease in the anthropogenic CO emissions seen in Europe and North America during the 1996–2006 period and a 20 % increase in the anthropogenic CO emissions in East Asia, during the same time period. The possible impacts of CH_4 and biogenic volatile organic compounds (BVOCs) are also considered. The European and global-scale EMEP models have been evaluated against the measured CO and C_2H_6 partial columns from Jungfraujoch, Zugspitze, Bremen, Harestua, Kiruna and Ny-Ålesund. The European model reproduces, on average the measurements at the different sites fairly well and within 10–22 % deviation for CO and 14–31 % deviation for C_2H_6. Their seasonal amplitude is captured within 6–35 % and 9–124 % for CO and C_2H_6, respectively. However, 61–98 % of the CO and C_2H_6 partial columns in the European model are shown to arise from the boundary conditions, making the global-scale model a more suitable alternative when modeling these two species. In the evaluation of the global model the average partial columns for 2006 are shown to be within 1–9 % and 37–50 % of the measurements for CO and C_2H_6, respectively. The global model sensitivity for assumptions made in this paper is also analyzed.

Correspondence to: J. Mellqvist
(johan.mellqvist@chalmers.se)

1 Introduction

During the last 30 years the trend in tropospheric carbon monoxide (CO) has turned from positive in the 1980s, to negative, in the 1990s and 2000s. The trend in the Northern Hemisphere has changed from approximately a 1 % increase per year to a decrease of 1–1.5 % per year with the strongest negative trends reported at high northern latitudes

(Khalil and Rasmussen, 1988, 1994; Novelli et al., 2003). In contrast, ethane (C_2H_6) has shown a constant negative trend in both the 1980s and 1990s of roughly 1–3 % per year (Rinsland et al., 1998; Mahieu et al., 1997).

These changes are important as tropospheric chemistry to a large extent is controlled by the hydroxyl (OH) radical, also often referred to as the detergent of the atmosphere. One of the main OH sinks is the reaction with CO (Crutzen et al., 1999). In this oxidation, the greenhouse gas carbon dioxide is formed but the reaction is also related to the formation or destruction of tropospheric ozone (O_3), depending on the NO_x concentrations in the ambient air. C_2H_6 is the second most common organic trace gas in the troposphere after methane (CH_4) and is, like CO, destroyed by the OH radical. C_2H_6 has also shown to be a major route for the formation of peroxyacetyl nitrate (PAN) which acts as a NO_x reservoir and thereby accelerates O_3 formation in the troposphere (Blake and Rowland, 1986; Finlayson-Pitts and Pitts, 2000).

Trends in the concentration of CO and C_2H_6 as seen from a particular location can result from both changes in emissions and changes in chemical production and loss processes. Observations alone cannot usually distinguish between these factors. In principal, chemical transport models (CTMs) can account for all the major processes affecting CO and C_2H_6, but such models are also limited by both inherent deficiencies and not least by the quality of the emissions data upon which such models rely.

The purpose of this paper is to make use of one such CTM to explore the trends seen in ground-based solar FTIR (Fourier Transform InfraRed) measurements of CO from four European stations. The model used is the global-scale model of the European Monitoring and Evaluation Programme developed by the Meteorological Synthesizing Centre – West (EMEP-MSC-W). The FTIR datasets used in this paper are compiled within the NDACC network (Network for the Detection of Atmospheric Composition Change, http://ndacc.org/) for which a wide range of atmospheric species is measured in the mid-infrared spectral region with high-resolution spectrometers, generally since the early 1990s, and even the mid-1980s at Jungfraujoch. An important part of the current study is also to evaluate how well the EMEP model reproduces observed CO and to a lesser extent C_2H_6 levels, both as an opportunity to evaluate this model using novel measurements, and to give confidence to the use of the model for such sensitivity analysis. It can be noted that many comparisons between CTMs and satellite and in situ measurements regarding CO have been performed but often with poor results, especially for the spring time maxima (Isaksen et al., 2009; Shindell et al., 2006).

2 Chemistry and sources of CO and C_2H_6

CO concentrations in the atmosphere are affected by emissions and chemical formation. Primary emissions of CO result from incomplete combustion of carbon-containing fuels. In developed countries the major anthropogenic source is related to emissions from the transport sector (Finlayson-Pitts and Pitts, 2000). Natural CO sources include oxidation from organics, primarily from atmospheric methane and biogenic hydrocarbons (BVOC), and from biological processes in soils and ocean. An overview of the estimated global CO sources is presented in Table 1. In Table 1 it can be seen that the major source for CO is the natural one and that the anthropogenic source globally only contributes to approximately 15 % of the total yearly emissions. Almost all of the CO emissions from fossil fuel combustion and 2/3 of those from biomass burning are located in the Northern Hemisphere (Holloway et al., 2000). The CO source from oxidation of biogenic hydrocarbons is roughly equally divided between the hemispheres and that from methane oxidation is slightly larger in the Northern Hemisphere. The major CO sink is the reaction with the OH radical, seen in Reaction (1), accounting for 90–95 % of the total CO loss (Lelieveld et al., 2002). CO is also a key compound in the formation and destruction of tropospheric O_3 depending on the background concentrations of NO_x (Crutzen et al., 1999).

$$CO + OH(+O_2) \rightarrow HO_2 + CO_2 \quad \text{(R1)}$$

In the Northern Hemisphere, Reaction (R1) is the dominant sink for OH, and even in polluted European boundary layers, CO accounts for a significant fraction of the OH loss (Simpson et al., 1995). The OH radical is produced from photodissociation of O_3 ($\lambda \leq 0.32$ µm) and reaction with water vapor according to Reactions (R2) and (R3), respectively. Since the formation of the OH radical is strongly dependent of the amount of sunlight, the CO concentration shows a strong intra-annual behavior with low values in the summer and high in the winter.

$$O_3 + h\nu \rightarrow O_2 + O(^1D) \quad \text{(R2)}$$

$$O(^1D) + H_2O \rightarrow 2OH \quad \text{(R3)}$$

In Reaction (R3) only a small fraction ($\sim$10 %) of the energetically excited oxygen atoms, $O(^1D)$, react with water molecules and produce OH, the others recombine with O_2 to form O_3 (Finlayson-Pitts and Pitts, 2000).

The main C_2H_6 source is of anthropogenic origin and includes production and transport of fossil fuels and use of biofuel. Another important source is biomass burning (Xiao et al. 2008, Table 1). Xiao et al. (2008) also estimate the anthropogenic and biomass burning emissions in Europe to be 2.1 and $<0.1\,\mathrm{Tg\,yr^{-1}}$, respectively. As much as 84 % of the C_2H_6 sources are located in the Northern Hemisphere, with highest emissions in Asia followed by North America

Table 1. Global sources of CO and C_2H_6 (Tg yr^{-1} and % of total). CO data are from Holloway et al. (2000) and C_2H_6 data are from Xiao et al. (2008).

	CO		C_2H_6	
Source	Tg yr^{-1}	%	Tg yr^{-1}	%
Anthropogenic*	408 (130-893)	15.1	8.5 (5-10.6)	64.9
Biomass burning	621 (310–920)	23.1	3.3 (1.3–6.4)	25.2
Biogenic hydrocarbon oxidation	530 (290–683)	19.7	Not a source	
Methane oxidation	910 (722–1459)	33.8	Not a source	
Biological processes	225 (0–756)	8.4	1.3	9.9
Total	2694 (1452–4711)	100	13.1 (6.3–17.0)	100

*Including: combustion, production and transportation of fossil fuels and combustion of bio-fuels

Table 2. Ground-based solar FTIR stations participating in the EMEP model comparison with available time period and number of measurements for each species.

Station	Latitude (° N)	Longitude (°E)	Altitude (m a.s.l.)	Retrieval code	Time period of data	Number CO	Number C_2H_6
Jungfraujoch	46.6	8.0	3580	SFIT2	1996–2006	1146	1175
Zugspitze	47.4	11.0	2960	SFIT2	1996–2006	736	671
Bremen	53.1	8.1	10	SFIT2	2002–2006	129	46
Harestua	60.2	10.8	600	SFIT2	1996–2006	458	507
Kiruna	67.8	20.4	420	PROFFIT	1996–2006	614	881
Ny-Ålesund	78.6	11.6	10	SFIT2	1996–2006	287	301

and Europe. The main sink, which causes up to 95 % of the C_2H_6 removal, is the reaction with the OH radical in which the ethyl radical and water are formed, see Reaction (R4).

$$C_2H_6 + OH \rightarrow C_2H_5 + H_2O \quad \text{(R4)}$$

The ethyl radical is then transformed through a complicated pattern of oxidations and reductions and ultimately ends up as CO (Aikin et al., 1982).

3 FTIR measurements

In this paper, FTIR partial column data of CO and C_2H_6 from six European stations are used from the time period of 1996–2006. Information regarding the FTIR stations can be found in Table 2.

A column is defined as the integrated amount of a species from the measurement station to a certain altitude, usually expressed as the number of molecules per unit area (molecules cm^{-2}). When retrieving data from solar FTIR measurements, a synthetic spectrum is calculated in a forward model in which the atmosphere is divided into discrete layers. To compute the synthetic spectrum, a priori vertical distributions, line parameters for the target and interfering gases, as well as temperature- and pressure profiles are needed. In the FTIR case line parameters from HITRAN are often used (Rothman et al., 2005). To account for the line broadening caused by the spectrometer, the instrument lineshape is included in the calculation. The synthetic spectrum is then compared with the measured one and the forward model parameters are adjusted in an iterative way until the modeled spectrum is sufficiently close to the measured one. This inverse process is an ill-posed problem that is solved in this paper with the Optimal Estimation Method (OEM) in which the final retrieved profile is a statistical weighted combination of an a priori profile of the target gas and the measurement (Rodgers, 2000). In order to use the OEM, uncertainties in the a priori profile and measurements have to be assumed/known. The partial column is obtained by multiplying the retrieved profile with a pressure profile and summing the result to the height of interest. The retrieval procedure is implemented in an algorithm called SFIT2 (Rinsland et al., 1998) which is used for all the participating stations except Kiruna, which uses PROFFIT (Hase et al., 2004). These two algorithms have shown to be within 1 % agreement (Hase et al., 2004; Duchatelet et al., 2010). The micro-windows used in the present retrievals are in the region from 2057 to 2159 cm^{-1} for CO and from 2976 to 2977 cm^{-1} for C_2H_6. For CO, the interfering species O_3, H_2O, CO_2, N_2O and OCS are fitted simultaneously, while CH_4, O_3 and H_2O are co-fitted in the C_2H_6 window. The retrieval strategy used for CO and C_2H_6 was developed within the UFTIR (http://www.nilu.no/uftir/) project and are further

described by De Maziere (2005) and Vigouroux et al. (2008). Error budgets of ground-based solar FTIR CO and C_2H_6 measurements has been reported by Zhao et al. (2002) for two Japanese stations and by Rinsland et al. (2000, 2007) for Jungfraujoch and Kitt Peak. The reported total errors for CO are between 5.2 % and 6.7 % and for C_2H_6 between 8.4 % and 8.9 %. The three papers have used the same microwindows, interfering species and retrieval algorithm (SFIT2) as in this paper but uses site specific a priori, pressure and temperature profiles. We conclude that the errors budgets from the references are applicable for the other stations used in this paper due to their varying altitude and latitude. The instrumental line shape, which is site specific, also affects the error. Although, the instrumental line shapes at all stations are monitored with gas cells measurements on a regular basis and the error is therefore assumed to be small. These measurement are retrieved with the LINEFIT program developed by Hase et al. (1999).

4 The EMEP model

The European Monitoring and Evaluation Programme (EMEP, www.emep.int) started in 1977, a successful effort between almost all European countries to pool efforts in tackling the major environmental problem of the day, acid deposition. When the Convention on Long-range Transboundary Air Pollution (CLRTAP, www.unece.org/env/lrtap) was established in 1979, EMEP became an integrated part of the Convention, and has since played an important part in the development of emission reductions scenarios, for both the Convention (now comprising 51 Parties, including USA and Canada) and the European Commission.

The EMEP chemical transport model (CTM) (Simpson et al., 2003a, 2010) is a development of the 3-D chemical transport model of Berge and Jakobsen (1998), extended with photo-oxidant chemistry (Simpson et al., 1995, 2003b; Andersson-Skold and Simpson, 1999) and the EQSAM gas/aerosol partitioning model (Metzger et al., 2002). Traditionally, this model has been run in a domain centered over Europe, but also covering large parts of the North Atlantic. The European-scale model has a resolution of about $50 \times 50\,km^2$, true at 60° N polar stereographic projection, and extending vertically from ground level to the tropopause and the lower stratosphere (100 hPa). The model has undergone substantial development in recent years, and is now applied on scales ranging from local (ca. 5 km grid size, Vieno et al., 2010) to global (with 1 degree resolution, Jonson et al., 2010). The model presented in this paper uses version rv3.5, see Simpson et al. (2010). Both natural and anthropogenic emissions are included. The anthropogenic emissions are provided by most European countries on the $50 \times 50\,km^2$ grid, otherwise derived from global databases or expert estimates. Biogenic emissions of isoprene in Europe are based on Guenther et al. (1993) and Simpson et al. (1999), driven by landcover for the appropriate grid. Emissions from forestfires are available as 8-day averages from the GFED (Global Emission Fire Database) database of van der Werf (2006). Unfortunately these data do not cover the full 1996–2006 period of our trend-runs, so we run the European-scale version of the model without forest fires, and evaluate their impact for 2006 with the global version.

For the global model, meteorological fields are derived from the European Centre for Medium Range Weather Forecasting Integrated Forecasting System (ECMWF-IFS) model (http://www.ecmwf.int/research/ifsdocs/). For the European scale, we here use the PARLAM-PS – a dedicated version of the HIRLAM (HIgh Resolution Limited Area Model) NWP, with parallel architecture (Källén, 1996; Lenschow and Tsyro, 2000). The performance of the EMEP model varies of course with the meteorological driver, but differences are modest for most pollutants, and affected mainly species subject to wet deposition or sensitive to near-surface dispersion, two factors that have little impact on column simulations of CO. Tarrason et al. (2008) discuss the differences in more detail, and Sect. 6 will present results from both European and global model versions for comparison.

When run at the European scale, initial and boundary values are required for the important long-lived pollutants, notably O_3, CH_4, CO and some hydrocarbons including C_2H_6. Concentrations of O_3 are most crucial to the model's photochemical calculations, and these are derived from climatological data of Logan et al. (1999), modified with a so-called Mace-Head correction to correct for observed monthly background O_3 changes (Simpson et al., 2003c). CO and C_2H_6 are specified as simple functions of latitude, altitude and time-of-year. The values were chosen to loosely reproduce observations from a number of studies (e.g. Derwent et al., 1998; Ehhalt et al., 1991; Emmons et al., 2000; Warneck, 2000) and the equations for the boundary condition calculations for CO and C_2H_6 are presented in Eqs. (1) and (2).

$$C_0 = C_{\mathrm{mean}} + \Delta C \cdot \cos\left(2\pi \frac{(d_{\mathrm{mm}} - d_{\mathrm{max}})}{n_{\mathrm{y}}}\right) \quad (1)$$

The CO and C_2H_6 concentrations at ground-level (C_0) are calculated as a function of the average concentration (C_{mean}), the amplitude (ΔC) and the phase where d_{mm} is the mid month number, d_{max} is the day at which C_0 maximizes and n_y is the number of days each year. Vertical (profile) concentrations are calculated according to Eq. (2), where h is the height and H_z is the scale height with, 10 km used for C_2H_6 and 25 km for CO.

$$C_i(h) = C_0 \exp(-h/H_z) \quad (2)$$

The parameters used in Eqs. (1) and (2) can be found in Simpson et al. (2003c).

The European EMEP model has been compared with observations and trends in several studies. Jonson et al. (2006) examined trends in ground-level ozone, Simpson

et al. (2006) looked at deposition fluxes of sulphur and nitrogen, Fagerli et al. (2007) compared historical trends of sulphate, ammonium and elemental carbon against ice-core records in the Alps, and Fagerli and Aas (2008) examined trends in nitrogen compounds in air and precipitation from 1980–2003.

In recent years the EMEP model has been extended to run at the hemispheric and global scales. Indeed, calculated results with an earlier hemispheric version of the model have been uploaded to the HTAP database (Hemispheric Transport of Air Pollution, www.htap.org). More than 30 models have uploaded model calculations for the year 2001 on this database, with model intercomparisons and comparison with measurements reported in several studies (HTAP, 2007; Fiore et al., 2009; Shindell et al., 2008; Sanderson et al., 2008; Reidmiller et al., 2009; Jonson et al., 2010). In general the EMEP model performs well compared to the other models in the database for surface species and depositions. In the free troposphere the EMEP model tended to underpredict ozone in the summer months compared to other models and to measurements (Jonson et al., 2006). For tropospheric CO, the EMEP results were at the high end of the ensemble of the hemispheric CO calculations. Since this HTAP study, changes have been made to the advection scheme (in particular with the inclusion of a convection scheme for dealing with e.g. sub-grid cumulus clouds), and ozone levels in the free troposphere are now higher, and in much better agreement with measurements (Jonson et al., 2010). These revisions have also led to substantially lower CO in the free troposphere, and results should now be close to the TF HTAP ensemble mean. (Within TF HTAP a new set of model calculations are planned for 2012. The EMEP model will take part in this model intercomparison). As the convective scheme is such a new addition to the EMEP model, and such schemes are more uncertain (Stevenson et al., 2006), we run here versions with and without the scheme.

Concerning emissions and chemical species, it should be noted that there is a large difference between CO and C_2H_6 in the model system. CO is a well-defined pollutant with its own emission databases. Such CO emissions data are thought to be fairly reliable over Europe and North America at least, although with larger uncertainties in other parts of the globe. On the other hand, C_2H_6 is a compound whose emissions are not explicitly mapped within the EMEP model. Instead, emissions of non-methane volatile organic compounds (NMVOC) are available, distributed in 10 so-called SNAP sectors, with e.g. SNAP4 representing production processes, SNAP5 extraction and distribution of fossil-fuels, SNAP7 representing motor vehicles, etc. For each of these SNAP categories we have a default speciation profile, in which the percentage of C_2H_6 is specified. This profile is largely based upon emissions data from the UK however (Passant, 2002), and its validity in other areas is questionable. As C_2H_6 has very particular emission sources which will not be captured by such a simple percentage-contribution system, e.g. from gas-leakage, it is actually unlikely that the model's emission inventory for this compound is of sufficient quality to derive a meaningful trend analysis. Further, the model's C_2H_6 is actually a surrogate compound, representing not just real C_2H_6 but also some other low-reactivity compounds. For these reasons we will present the FTIR trends of CO and C_2H_6, but concentrate on the modeled trends of CO.

5 Method

The European-scale version of the EMEP model is first run over the time-period 1996–2006. These runs are intended to firstly evaluate the model's CO and (to a lesser extent) C_2H_6 fields, and secondly to determine the extent to which the changes in emissions and chemistry over the European domain can account for changes observed in the FTIR network. The global-scale EMEP model is essentially the same as the European-scale model, but not so dependent on initial and external boundary conditions, and driven by a different meteorological driver. As well as accounting for intercontinental transport, the global model is also able to account for recirculation of those air masses from Europe which pass beyond the boundaries of the European model. A comparison of the global model against FTIR measurements and the European model is also performed. The global-scale model is then used in a series of sensitivity scenarios to investigate possible cause for the CO trends seen in the FTIR measurements. The model versions and sensitivity scenarios are summarized in Table 3.

5.1 Calculations of partial columns

Since both the European and global-scale EMEP model domains only extend up to 100 hPa, whereas the FTIR data extends throughout the whole atmosphere, partial columns from the FTIR measurements have to be derived for comparability. The partial columns consist of the tropospheric columns and those parts of the stratospheric columns that are below 100 hPa. These are simply calculated by subtracting the average part of the total columns above 100 hPa from the total columns. The averages are based on the retrieved FTIR profiles from Harestua and Jungfraujoch in the CO case and Harestua in the C_2H_6 case. The CO average is $6.1 \pm 2.2 \times 10^{16}$ molecules cm^{-2} and the C_2H_6 average is $5.0 \pm 2.2 \times 10^{14}$ molecules cm^{-2}, corresponding to ∼3–6 % and ∼2 % of the total columns for each species, respectively. The uncertainties are presented on a 2-σ level. FTIR partial columns, in this case above 12 km, have earlier been reported to be at most 10 % and 7 % of the total column for CO and C_2H_6, respectively (Zhao et al., 2002).

The EMEP model data was obtained from discrete constant layers for both the European and global-scale models. To adjust the model to the actual altitude of the FTIR measurement stations, a linear interpolation, based on the

Table 3. EMEP model versions and sensitivity scenarios used in this paper.

EMEP model versions	Short name
European model	E
Global model	G
Global model with convection	Gc
As Gc but with forest fire module	Gcff
Sensitivity scenarios (based on the Gc model version)	**Short name**
20 % reduction of European anthropogenic CO	GcEUR20
20 % reduction of North American anthropogenic CO	GcNA20
20 % increase of East Asian anthropogenic CO	GcEA20
20 % reduction of all European emissions	GcEURAll20
20 % reduction of all North American emissions	GcNAAll20
20 % increase of all East Asian emissions	GcEAAll20
0.2 °C increase of the global temperature	GcT0.2
1.2 % increase of global CH_4	Gc$CH_4$1.2
100 % reduction of North American BVOC	Gcnobvoc

difference between the station altitude and average topographical altitude in the grid area used by the EMEP model, was applied. Fagerli et al. (2007) discussed this issue in more detail, but for this exercise, the simple height-based interpolation is assumed to be sufficient for the model evaluation. The trend sensitivity study is not affected by the model baseline, i.e. the interpolation, since it is based on relative changes.

5.2 Trends and tracers

The FTIR trends are estimated with a method developed by Angelbratt et al. (2011). The method is based on multiple linear regressions where other data such as surface pressure and total column of hydrogen fluoride (HF) are used to reduce the variability in the FTIR time series and thereby explain part of the atmospheric dynamics resulting, for example, from tropopause changes or from the presence of the polar vortex. The model also contains a function that captures the seasonal fluctuations and the linear trend. Trends are estimated from the EMEP model by using simple linear regression. When estimating confidence intervals for the trends both of the above-mentioned methods assume that the residuals (data minus trend model) are normal distributed, are free from auto-correlation and have equal variance around zero. The method of confidence interval on individual regression coefficients described in Montgomery et al. (2008) is used. Trends are not estimated for Bremen due to the short time series and Ny-Ålesund due to the lack of measurements during winter.

Tracers for CO and C_2H_6 have been introduced into the EMEP model, in order to track concentrations originating from the boundary and initial conditions (BICs). Tracers are lost to OH using the same rates as for CO and C_2H_6, but the tracers do not influence the chemical simulations. Thus, at the start of the simulation the modeled concentrations of CO and C_2H_6 are identical to their tracer counterparts. As the simulation proceeds, emissions and chemical production and loss affect the real species, but the tracers respond only to advection and chemical loss. As the European-scale model has a limited spatial domain it can be heavily influenced by BICs, so that the tracer concentrations frequently amount to a large percentage of the real concentrations. The global-scale model is mainly influenced at the start of the simulation (see Sect. 6).

5.3 Sensitivity analysis for CO trends

To find possible causes for the estimated CO trends in the FTIR dataset, see Sect. 6.1.2, a series of sensitivity scenarios are tested in the global-scale model; the scenarios are summarized in Table 3 and are described in detail below. As a baseline-simulation we use the standard model, with convection, but without forest fires (Gc) and all the sensitivity scenarios are compared with this simulation. The scenarios have been chosen to loosely represent known emission changes or climate effects and the mass balance is schematically described in Eq. (3), where P represents the production terms and D the destruction of CO in Tg yr^{-1}. In this paper, $P_{\text{Anthropogenic}}$ is defined as the CO emissions, mainly from combustion in industrial processes and the transport and energy sector while forest fires, savannah and agricultural waste burning are included in the $P_{\text{Biomassburning}}$ term. The $P_{\text{CH4oxidation}}$ and $P_{\text{BVOCoxidation}}$ are defined as the formation of CO from the oxidation of these species with the OH radical. CO can also be formed in biological processes in soils and oceans and these comprise the $P_{\text{Biological}}$ term in Eq. (3). The main sink of CO is the reaction with the OH radical and thereby the destruction term D_{OH}.

$$\text{Trend} = P_{\text{Anthropogenic}} + P_{\text{Biomass burning}} + P_{\text{CH4 oxidation}} + P_{\text{BVOCoxidation}} + P_{\text{Biological}} - D_{\text{OH}} \quad (3)$$

In the first two scenarios a reduction of anthropogenic CO emissions by 20 % in Europe and North American are tested (GcEUR20 and GcNA20) and this corresponds to a decrease per year of ∼2 % during the 11-year period of 1996–2006 for which the FTIR measurements are taken. In Monks et al. (2009) and the EDGAR database v. 4.0 (2009) the anthropogenic CO emissions in Europe have been shown to decrease by 1.7 % yr^{-1} to 4.5 % yr^{-1} and the North American emissions have been show to decrease by 2.1 % yr^{-1} to 3.7 % yr^{-1}, where the trends are based on data from the late 1990s and early 2000. The reported emission reductions for both continents indicate that our reduction of 2 % yr^{-1} is a reasonable value to use in the two sensitivity scenarios. Further, we have decided to use a reduction in the lower range for both of the scenarios so the change in the modeled CO partial columns is not overestimated.

Unlike North America and Europe, many countries in Asia have increased their CO emissions during the last decades. In the third scenario (GcEA20) we investigate how a 20 % increase in the East Asian anthropogenic CO emissions is affecting the CO trends seen in Europe. We define East Asia as China and Japan, and for model simulations use the same area as defined by Fiore et al. (2009). According to Monks et al. (2009), China has increased its CO emissions by approximately 15 % from 1996 to 2003 where the years after 2000 shows the strongest increase. Data from the EDGAR emission database v.4.0 (EDGAR, 2009) show a 24 % increase for China and a 4 % decrease for Japan from the 1996 to 2005 time period. The reported emission data from China and Japan indicate that a 20 % increase during the 1996–2006 period is a reasonable assumption.

In scenarios four and five, GcEurAll20 and GcNAAll20, the emissions from all anthropogenic sources (CO, NO_x, NMVOC, SO_x, and NH_3) are reduced by 20 % for Europe and North America (again using the Fiore et al. (2009) domain definitions). Since both CO and the other species have decreased, these scenarios illustrate more realistic situations where the chemical interactions between the species are included in the simulation. Scenario six corresponds to a 20 % increase for the same species as in four and five but for East Asia (GcEAAll20).

In scenario seven the global surface temperature as used in the BVOC calculations are increased by 0.2 °C (GcT0.2). According to Hansen et al. (2006) the global temperature has approximately increased by 0.2 °C over the study period presented in this paper and since the BVOC emissions are strongly temperature dependent, such emissions should also have increased.

In the last sensitivity scenario (Gc$CH_4$1.2) it is investigated how the partial columns of CO are affected by the methane (CH_4) concentrations. Both surface concentration and total column measurements of CH_4 have been shown to increase from 1996 to 1999 and thereafter flatten out towards a zero trend for the rest of the studied period (Dlugokencky et al., 2009; Angelbratt et al., 2011). The average increase over the first three years was 0.4 % yr^{-1}. A proper modeling assessment of these CH_4 changes would need to run over many years because of the lifetime of CH_4 (∼10 years) (Fiore et al., 2009). Here we make a first order approximation and calculate the effect of a single 1.2 % yr^{-1} emission change calculated over one year (2006).

5.4 Uncertainty analysis

A number of other tests have been conducted with the global model, which explores the importance of some model assumptions. As noted in the introduction, the convection routine is new to the EMEP model and optional. Although convection is unquestionably important to atmospheric transport, the parameterization of this in models is also quite uncertain (Stevenson et al., 2006). For this reason we have run a model version (G, Table 3) without convection. A second test with the global model is the introduction of forest-fire emissions. Although such emissions should in principal be part of a default model run, we only have 8-day average emissions. Thus, when comparing with daily FTIR data, we have chosen to omit these data from the baseline-case, but in test Gcff forest-fire emissions are added for comparison. As discussed in Sect. 5.1 (Fagerli et al., 2007), model results are derived as an interpolation between discrete model layers, and some uncertainty is associated with this procedure. Two tests (Gc-high, Gc-low, Table 3) are conducted in which the model results are taken from model-layers higher than, or lower than, this default. The uncertainty in the derived partial columns, Sect. 5.1, is investigated in two tests, FTIR-high and FTIR-low. Finally, we have conducted one more, extreme, test of the BVOC emissions, namely setting all such emissions to zero (Gcnobvoc). This test is designed purely to explore the magnitude of CO associated with BVOC emissions. Such emissions are in fact one of the most uncertain inputs to the CTMs, at least over North America and Europe where other emissions are known with reasonable accuracy, and according to Granier et al. (2000), BVOC contribute up to 18 % of the global budget of CO. Simpson et al. (1999) estimated a factor 2–3 uncertainty for European isoprene emissions (and much worse for other BVOC), and Warneke et al. (2010) found factor of two differences between two BVOC inventories in the United States, with measurement-based data unable to distinguish which was best.

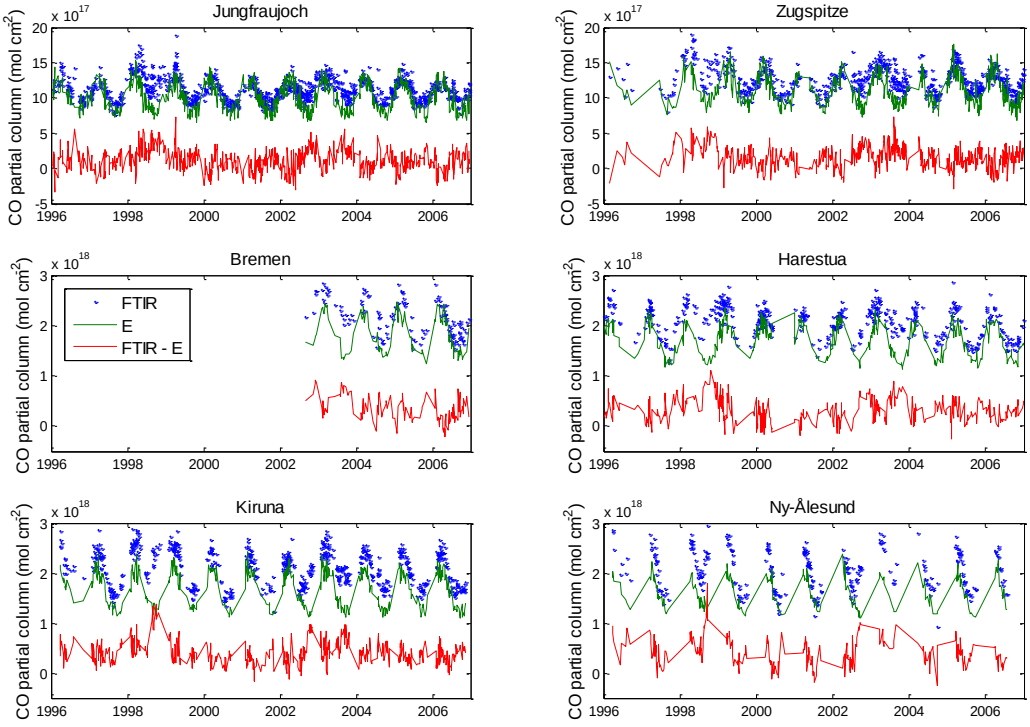

Fig. 1. CO comparison between European EMEP model (E) and FTIR measurements. The measurements are marked as dots and the model is marked as a solid green line. The difference between measurements and model is marked as a red solid line.

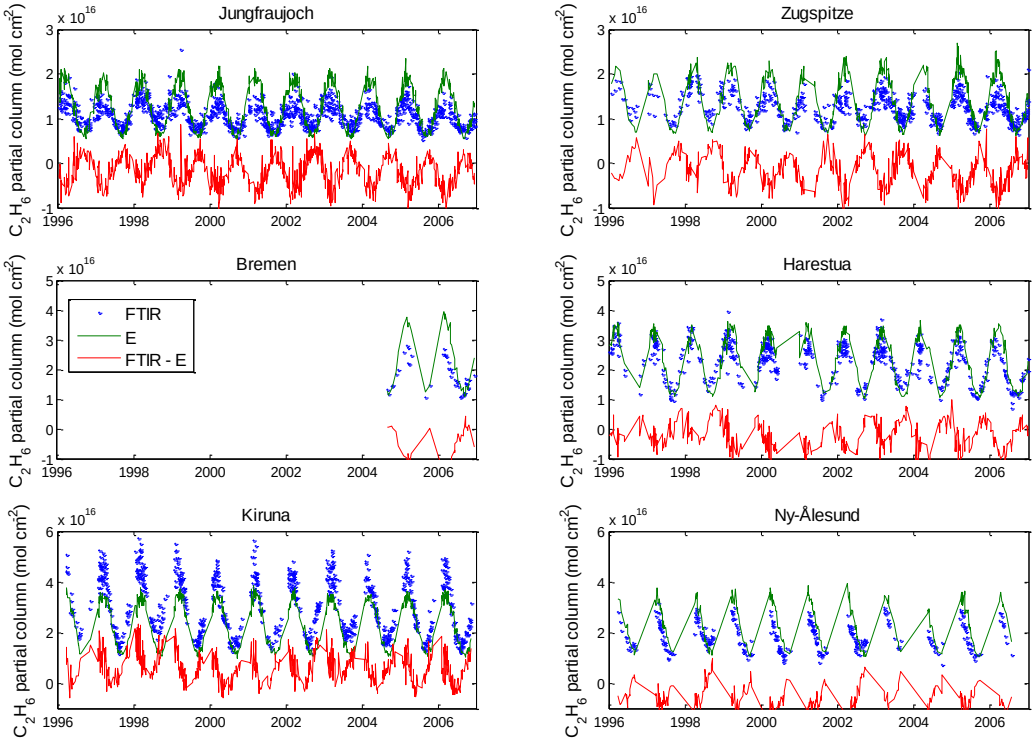

Fig. 2. As in Fig. 1 but for C_2H_6.

Table 4. Average values (μ), standard deviations (σ) and seasonal amplitudes (A) from the FTIR measurements and European-scale model (E). A is the difference between the average values of March and April and July to September.

	CO (molecules cm^{-2} × 10^{17})						C_2H_6 (molecules cm^{-2} × 10^{15})					
	FTIR			E			FTIR			E		
	μ	σ	A	μ	σ	A	μ	σ	A	μ	σ	A
Jungfraujoch	11.1	1.6	1.4	10.0	1.9	1.9	10.7	2.7	2.5	12.5	4.7	5.6
Zugspitze	12.6	1.8	1.6	11.0	2.1	2.0	12.5	3.0	2.9	14.2	5.2	6.3
Bremen	21.5	3.5	2.9	18.1	3.6	3.5	17.6	5.1	5.1	22.6	10.0	10.4
Harestua	21.0	3.0	3.1	17.8	3.1	3.3	23.4	6.4	7.1	25.8	7.8	9.5
Kiruna	21.2	3.5	3.2	17.0	3.5	3.4	30.6	11.4	11.0	24.2	9.3	10.0
Ny-Ålesund	20.6	4.0	3.8	16.3	2.9	3.3	18.4	5.5	6.0	24.1	8.2	9.7

Table 5. Average (μ) and standard deviation (σ) contribution from the boundary conditions (BIC) for the European-scale EMEP model, expressed in percent (%).

	CO		C_2H_6	
	μ	σ	μ	σ
Jungfraujoch	65.8	18.4	76.2	14.8
Zugspitze	61.4	15.6	74.4	12.6
Bremen	60.8	15.5	71.2	14.3
Harstua	72.5	14.8	78.5	14.1
Kiruna	87.6	12.5	91.8	9.7
Ny-Ålesund	96.6	5.1	98.2	3.6

6 Results and discussion

6.1 European model 1996–2006

6.1.1 Average partial column and seasonal amplitude

The comparison of the European-scale model with the CO and C_2H_6 FTIR measurements is presented in Figs. 1 and 2, respectively. In general, strong similarities between the model and measurements can be seen for both species. To quantify the differences, average values, standard deviations and seasonal amplitudes are calculated for the two species, and are presented in Table 4. Compared to the low-level sites, the Alpine stations have a lower average partial column and seasonal amplitude due to their high altitude since a large part of the partial column is located below the station.

As noted in Sect. 4, the European-scale model uses climatological (monthly) BICs for CO and C_2H_6, and these values strongly determine the model's concentrations, and hence are responsible for much of the good agreement. The BIC influence is quantified by tracers and those are presented in Table 5, where it can be seen that columns at the modeled stations close to the model horizontal boundary are dominated by the BICs, while columns at the stations further away from the boundary include more information generated within the model. It can also be seen that more information is from the BICs for C_2H_6 than for CO.

A clear difference in CO between the model and the measurements can be seen in the years 1998 and 2002/2003 for most of the stations and this is particularly visible at Jungfraujoch and Kiruna in 1998. For C_2H_6 these differences are not so clear although they can be seen for example at Jungfraujoch and Kiruna in 1998. During these two time periods, large scale forest fires were present in North America and Russia and the CO contributions to the atmosphere were captured by the FTIR measurements (Yurganov et al., 2004, 2005). As noted in Sect. 4, forest fire emissions were not available at consistent time-resolution over the 11 years of this study, and so were omitted from the European-scale calculations. Furthermore, and probably most importantly, the model domain does not include North America and non-European parts of Russia and is hence highly dependent on the lateral boundary conditions.

Compared to the measurements, the model shows a slight phase shift for all the participating stations regarding CO and C_2H_6. For CO, the model tends to overestimate the seasonal amplitude and underestimate the average partial column. For C_2H_6, on the other hand, the model overestimates both the average partial column and seasonal amplitude and deviates from the FTIR data by as much as a factor of two. For both species, the model captures the inter-station variability quite well for both the average partial columns and the seasonal amplitudes. Although C_2H_6 has much less importance for EMEP modeling purposes (usually aimed at boundary layer ozone, or acidification and health issues) than CO, these results suggest a need to modify the global boundary conditions for the European EMEP model, and to re-evaluate the emission inventories for this compound.

6.1.2 Trends

All FTIR stations show significant negative CO trends on the 2-σ level, as presented in Table 6. For the 1996 to 2006 time

Table 6. Linear trends estimated from the partial columns (below 100 hPa) of CO and C_2H_6 from FTIR measurements. The trends are presented with their 2-σ confidence intervals and used the average value of 2001 as reference.

Station	Time period	FTIR trends (% yr^{-1})	
		CO	C_2H_6
Jungfraujoch	1996–2006	-0.45 ± 0.16	-1.51 ± 0.23
Jungfraujoch	1998–2006	-1.32 ± 0.20	-2.14 ± 0.29
Zugspitze*	1996–2006	-1.00 ± 0.24	-2.11 ± 0.30
Zugspitze	1998–2006	-1.16 ± 0.26	-2.25 ± 0.35
Harestua	1996–2006	-0.62 ± 0.19	-1.09 ± 0.25
Kiruna	1996–2006	-0.61 ± 0.16	-1.15 ± 0.18

* No CO data is available for Zugspitze from September 1996 to June 1997.

Table 7. Average values (μ) from March to December for the FTIR measurements, global-scale (Gc) model and European-scale (E) model. January and February data are excluded from the μ values because of the strong influence from the initital conditions in the global model.

	CO μ (mol cm^{-2} $\times 10^{18}$)			C_2H_6 μ (mol cm^{-2} $\times 10^{15}$)		
	FTIR	Gc	E	FTIR	Gc	E
Jungfraujoch	1.0	1.0	1.1	12.4	7.5	9.8
Zugspitze	1.1	1.2	1.2	14.2	9.0	11.6
Bremen	1.8	1.7	2.0	21.9	11.0	16.9
Harestua	1.6	1.6	1.9	21.9	12.9	18.9
Kiruna	1.6	1.6	2.0	23.3	13.6	27.9
Ny-Ålesund	1.8	1.7	2.1	29.9	17.7	21.9

period, Harestua and Kiruna are in close agreement to each other while the trends at Jungfraujoch and Zugspitze deviate more than expected, given their close geographical and altitude location. Compared to Jungfraujoch, Zugspitze has very few measurements in 1996 and 1997; this together with the unusually high values in 1998 and 1999 is probably one of the reasons for the strong negative trend at Zugspitze. The explanation is strengthened by the estimated trends from the 1998 to 2006 time period, where the trends are in much closer agreement for the two stations. Earlier, Zhao et al. (2002) have reported CO trends for the time period 1995–2000 of -2.1 ± 0.2 % yr^{-1} from FTIR tropospheric columns measured at two Japanese stations. Novelli et al. (2003) have reported an average trend from 1991-2001 for the Northern Hemisphere, from a network of flask sample measurements, of -0.92 ± 0.15 % yr^{-1}. Gardiner et al. (2008) have reported insignificant FTIR total column trends for Europe of -0.1 ± 0.46 % yr^{-1} to -0.58 ± 0.69 % yr^{-1}, this based on data from 1995–2004. Gilge et al. (2010) have reported in situ trends for the time period of 1996–2007 for Jungfraujoch and 1995–2002 for Zugspitze of roughly -2.1 ± 0.7 % yr^{-1}. The earlier reported trends and the ones presented in this paper indicate the presence of a negative trend in the Northern Hemisphere, although with a magnitude depending on the geographical location of the measurement station, the covered time period and the type of measurement.

Significant negative C_2H_6 trends are estimated for all FTIR stations, see Table 6. The trends are stronger compared to those of CO and vary from -2.25 ± 0.35 % yr^{-1} to -1.09 ± 0.25 % yr^{-1}. Again Harestua and Kiruna are in close agreement and Jungfraujoch and Zugspitze differ despite their proximity. To the author's knowledge, very few trend estimations have been performed for C_2H_6. Except the negative trends of 1.20 ± 0.35 % yr^{-1} and 2.70 ± 0.30 % yr^{-1} given in Rinsland et al. (1998) and Mahieu et al. (1997), the trends in this paper could be compared with the solar FTIR trends from 1995 to 2004 of: -0.63 ± 0.37 % yr^{-1} from Kiruna, -0.65 ± 0.32 % yr^{-1} for Harestua, -1.14 ± 0.60 % yr^{-1} for Zugspitze and -1.05 ± 0.35 % yr^{-1} for Jungfraujoch, presented by Gardiner et al. (2008).

No significant trends for CO and C_2H_6 have been found in the European-scale EMEP model. Since the model boundary conditions do not contain any trend components and most of the information at each station comes from the boundary conditions, see Table 5, we conclude that the model domain is too small for detecting trends from species with a lifetime as long as two months. To model a more realistic alternative regarding CO trends, the global-scale model will be used in Sect. 6.2.2.

6.2 Global model 2006

6.2.1 Evaluation of global-scale model

The comparison of the global and European-scale model with the FTIR measurements for 2006 is presented in Figs. 3 and 4 for CO and C_2H_6, respectively. The average values for each station and species are presented in Table 7.

The global-scale model reproduces the FTIR data slightly better than the European model for the partial columns of CO at all participating stations. The biggest difference is at the stations located at higher latitudes where the European model tends to overestimate the partial columns while the global model is in good agreement with the measurements. The overestimation by the European model at high latitudes is probably due to the high influence from the boundary conditions at these locations. Both the global and European model have problems reproducing the partial columns of C_2H_6. The global model significantly underestimates the partial columns at all stations and for some by as much as a factor of two. The European model also underestimates the partial column but not as much as the global model.

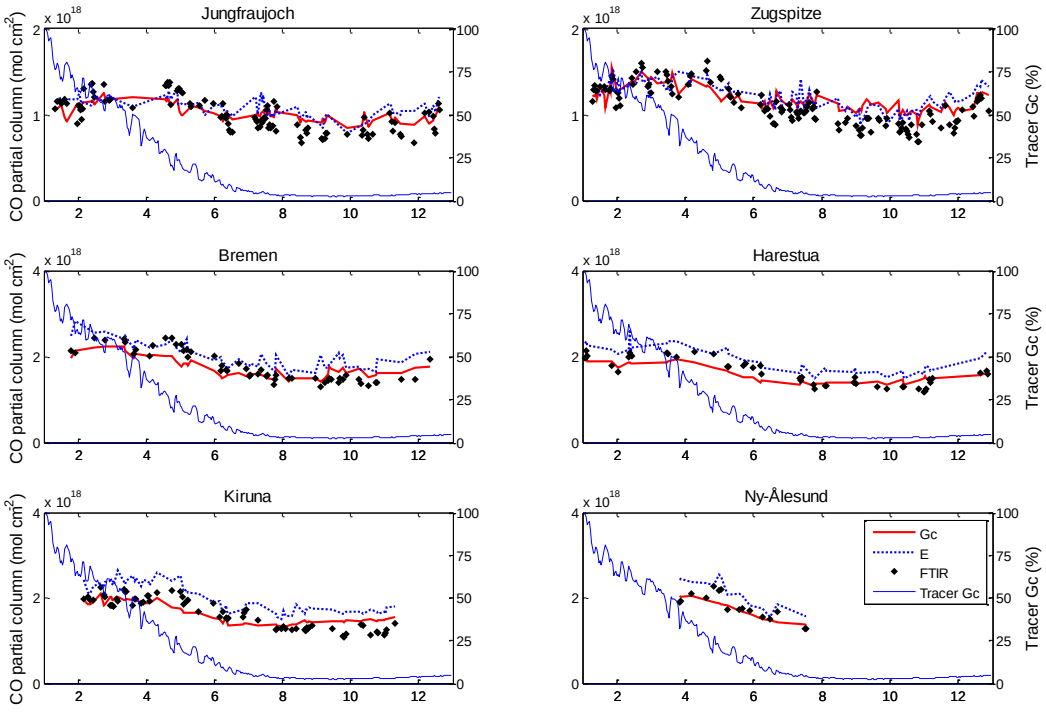

Fig. 3. CO partial columns of 2006 derived from the global (Gc) and European-scale (E) model. The FTIR and tracer calculations for the Gc model is also shown. The x-axis present months where zero refers to 1 of January. The first months are highly influenced by the model initial conditions which corresponds well to the CO and C_2H_6 lifetimes of 2–3 months (Finlayson-Pitts and Pitts, 2000).

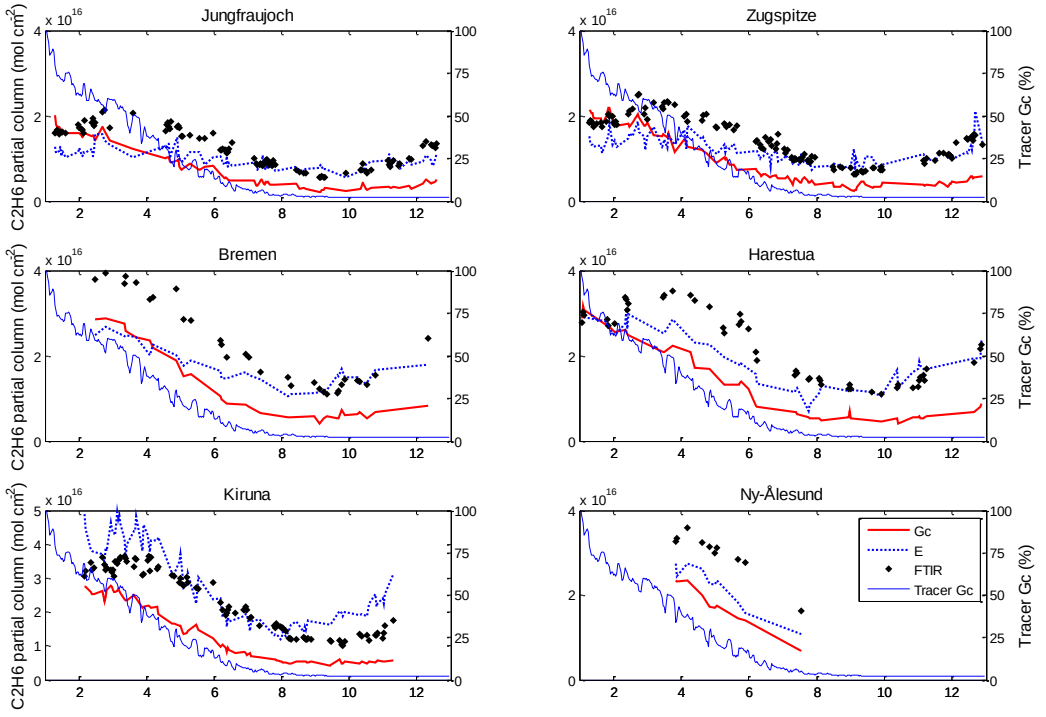

Fig. 4. As in Fig. 3 but for C_2H_6.

Table 8. Change in the CO partial column per year through the 1996–2006 time period. All the simulations are done on year 2006 and are scaled to represent the yearly change. No FTIR trends are estimated for Bremen and Ny-Ålesund due to the short time series and lack of winter measurements.

	Sensitivity cases (% yr^{-1})						
	GcEUR20	GcNA20	GcEA20	GcT0.2	$GcCH_4$1.2	ΣGc	FTIR
Jungfraujoch	−0.47	−0.22	0.15	0.04	0.13	−0.37	-0.45 ± 0.16
Zugspitze	−0.58	−0.21	0.15	0.04	0.13	−0.47	-1.00 ± 0.24
Bremen	−0.83	−0.21	0.15	0.04	0.13	−0.72	N/A
Harestua	−0.67	−0.21	0.16	0.04	0.13	−0.55	-0.62 ± 0.19
Kiruna	−0.60	−0.21	0.16	0.04	0.12	−0.49	-0.61 ± 0.16
Ny-Ålesund	−0.53	−0.20	0.18	0.04	0.12	−0.39	N/A

6.2.2 Sensitivity of CO trends

The outcome of the global-scale model sensitivity scenarios for CO is presented in Table 8 as percent change per year for each of the participating stations. The outcome is based on average values of all sensitivity and baseline scenarios where January and February data is removed due to the high influence from the initial conditions. The differences between the baseline scenario and the sensitivity scenarios is then scaled with the 11 year period (1996–2006).

The European anthropogenic CO reduction by 20 % (GcEUR20) has the largest impact on the modeled partial columns of all scenarios and could by itself account for a negative trend of 0.47–0.83 % yr^{-1}. Also, a 20 % reduction in the North American anthropogenic CO emissions (GcNA20) causes negative trends in the modeled partial column from 0.20–0.22 % yr^{-1}. The increase in the East Asian anthropogenic CO emission by 20 % (GcEA20) gives a positive contribution to the modeled European partial column trends of 0.15–0.18 % yr^{-1}; this region has a slightly smaller impact on the absolute European trends than North America. A global increase in the CH_4 column ($GcCH_4$1.2) and an increase in the global temperature by 0.2 °C during the 11-year period give a positive contribution to the modeled trends of $\sim$0.15 % yr^{-1} for all stations. Although these two scenarios are rough estimations, this highlights the fact that CO seems to be sensitive to both the global temperature and the CH_4 concentration.

When adding the five sensitivity scenarios discussed above (shown as ΣGc in Table 8), Jungfraujoch, Harestua and Kiruna have modeled trends that are close to the measured trends, while the modeled trend at Zugspitze deviates by a factor of two from the measured trends. The modeled trends follow the measured trends with a smaller trend at Jungfraujoch and larger trends at Harestua and Kiruna. It can also be seen that the modeled trend at Zugspitze is larger than the trends for Jungfraujoch. To exclude the altitude difference between the stations as a reason for this behavior, the trends at the ground layer are also modeled; this is presented in Table 9. In the comparison it can be seen that the trend difference is 0.07 % yr^{-1} at the ground while it is 0.10 % yr^{-1} when adjusting for the station levels. From this we conclude that the modeled trend difference between Jungfraujoch and Zugspitze is not due to the different altitudes of the stations but rather has to do with the origin of the air masses at each station. This fact might also be an additional explanation for the measured trend difference between Jungfraujoch and Zugspitze, presented in Sect. 6.1.2. The modeled trends at Bremen and Ny-Ålesund stands out a bit compared to the other stations. The small trend at Ny-Ålesund is not surprising since the station is located in the far north and is hence less affected by the European CO reduction. Bremen on the other hand has a central location and is affected by European CO reductions for all wind directions.

Table 9. Modeled trends at ground level and adjusted altitude.

	Sensitivity cases (% yr^{-1})	
	ΣGc altitude adjusted	ΣGc ground level
Jungfraujoch	−0.37	−0.60
Zugspitze	−0.47	−0.67

The 20 % reduction and increase in emissions of all anthropogenic species (GcEURAll20, GcNAAll20, GcEAAll20) represents the change in OH chemistry that occurs due to a change in the NO_x, NH_3, NMVOC and SO_x concentrations and thereby the assumed change in the CO partial columns. It was shown that the difference between the Gc20 and Gc20All scenarios hardly differs at all between the model calculations for the three regions. Since OH affects the CO concentrations both as (1) a sink and (2) a source through the oxidation of VOCs and CH_4, it turns out that these two processes cancel out each other and that the modeled CO partial columns are almost insensitive to changes in NO_x, NH_3, NMVOC and SO_x.

When considering the mass balance for CO in Eq. (3) we have investigated the presence of trends in three sources,

namely: anthropogenic CO emissions, oxidation of CH_4 and BVOC (through the GcT0.2 scenario). Possible trends in biomass burning and in the OH radical concentration due to factors other than the emission changes explored above have not been taken into account. Both the OH radical and biomass burning have large inter-annual fluctuations, this is for example shown by Yurganov et al. (2004, 2005) and Montzka et al. (2011), and these fluctuations contribute to the uncertainties in the estimated FTIR trends. To outline the effect on the CO trends of possible changes in the OH radical and biomass burning further studies are needed.

6.2.3 Uncertainty analysis

As discussed in Sect. 5.4, we have conducted a number of tests designed to quantify some of the uncertainties in the calculations, concerning convection, forest-fires and BVOC emissions as well as uncertainties related to the derivation of partial columns from the FTIR measurements (FTIR high and low) and the interpolation between the model layers (Gc high and low). In Fig. 5 the results of these tests are illustrated for Harestua, the results are similar for the other stations participating in this study. It can be seen that the model with the forest fire module (Gcff) in general reproduces the FTIR measurements best compared to the other two versions (G and Gc) where G is close to Gcff while Gc is underestimating the measurements. This illustrates that the convection module decreases the estimated partial columns while the forest fire module increases the partial columns and that the two modules together almost cancel out each other. It is also seen that the derivation of the partial columns from the FTIR measurements is almost insensitive to the seasonal variation of the 100 hPa level. This is not unexpected since a very small fraction of the partial column is located around this level. The model-FTIR comparison is more sensitive to the interpolation between the layers and the BVOC emissions and when removing all North American BVOC emissions a large underestimation of the partial columns of CO is seen.

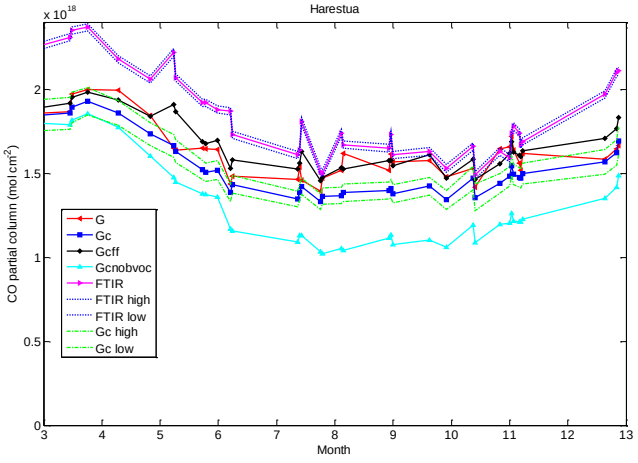

Fig. 5. Uncertainty analysis for the global-scale EMEP model performed at Harestua data. Except three model versions the interpolation limits for the model with convection is presented (Gc high and low), the FTIR upper and lower uncertainties for the partial columns (FTIR high and low) and one sensitivity scenario when all North American BVOC is removed (Gcnobvoc).

7 Conclusions

In this paper we have shown negative linear trends from partial columns of CO and C_2H_6 measured with the ground-based solar FTIR technique at four European stations, Jungfraujoch, Zugspitze, Harestua and Kiruna, from the time period of 1996–2006. The negative CO trends vary from $0.45 \pm 0.16\,\%\,yr^{-1}$ at Jungfraujoch to $1.00 \pm 0.24\,\%\,yr^{-1}$ at Zugspitze and to $\sim 0.60 \pm 0.20\,\%\,yr^{-1}$ at both Harestua and Kiruna. A similar pattern can be seen in the negative C_2H_6 trends but here the trends are stronger and cover a range from $1.09 \pm 0.25\,\%\,yr^{-1}$ to $2.11 \pm 0.30\,\%\,yr^{-1}$. All the estimated trends are significant on a 2-σ level, indicating that a decrease in the two species has occurred in Europe during the 1996–2006 period. To outline possible reasons for the measured negative CO trends the global-scale EMEP model was used in a series of sensitivity scenarios. It was found that the reduction in the European anthropogenic CO emissions during the 1996–2006 period could, to a large extent, explain the negative trends measured at the FTIR stations. Also, the decrease in North American and increase in East Asian anthropogenic CO emissions affected the measured CO partial columns in Europe but to a smaller extent than the European emission reduction. This paper should be considered as a first attempt to explain the CO trends seen in the FTIR measurements. Meteorology for the global-scale EMEP model was only available for 2006, the analysis can be improved in future if meteorology becomes available for the whole time period (1996–2006). Furthermore, of great interest is the effect of the variations in the OH radical and biomass burning on the trends in CO. This has been outside the scope of this article and a more detailed analysis, on a statistical basis, is needed to quantify the exact reasons for the measured trends.

Acknowledgements. The authors would like to thank the EU projects UFTIR and HYMN and the Swedish Environmental Protection Agency for financial support. Further, Anders Strandberg, Elisabeth Unden and Glenn Persson are thanked for measurement and data retrieval support. University of Liège was supported by the Belgian Science Policy Office (PRODEX and SSD programs) as well as by the European Union projects mentioned here above. We are grateful to the many colleagues who contributed to the FTIR data acquisition at the Jungfraujoch and would like to thank the International Foundation High Altitude Research Stations Jungfraujoch and Gornergrat (HFSJG, Bern) for supporting the facilities needed to perform the observations. The work of David Simpson was further supported by the EU 6th Framework Programme EUCAARI project (contract 036833-2), as well as

by Cooperative Programme for Monitoring and Evaluation of the Long-Range Transmission of Air Pollutants in Europe (EMEP) under UNECE.

Edited by: A. S. H. Prevot

References

Aikin, A. C., Herman, J. R., Maier, E. J., and Mcquillan, C. J.: Atmospheric Chemistry of Ethane and Ethylene, J. Geophys. Re., 87, 3105–3118, 1982.

Andersson-Skold, Y. and Simpson, D.: Comparison of the chemical schemes of the EMEP MSC-W and IVL photochemical trajectory models, Atmos. Environ., 33, 1111–1129, 1999.

Angelbratt, J., Mellqvist, J., Blumenstock, T., Borsdorff, T., Brohede, S., Duchatelet, P., Forster, F., Hase, F., Mahieu, E., Murtagh, D., Petersen, A. K., Schneider, M., Sussmann, R., and Urban, J.: A new method to detect long term trends of methane (CH_4) and nitrous oxide (N_2O) total columns measured within the NDACC ground-based high resolution solar FTIR network, Atmos. Chem. Phys., 11, 6167–6183, doi:10.5194/acp-11-6167-2011, 2011.

Berge, E. and Jakobsen, H. A.: A regional scale multi-layer model for the calculation of long-term transport and deposition of air pollution in Europe, Tellus B, 50, 205–223, 1998.

Blake, D. R. and Rowland, F. S.: Global Atmospheric Concentrations and Source Strength of Ethane, Nature, 321, 231–233, 1986.

Crutzen, P. J., Lawrence, M. G., and Pöschl, U.: On the background photochemistry of tropospheric ozone, Tellus A, 51, 123–146, 1999.

DeMazière, M., Vigouroux, C., Gardiner, T., Coleman, M., Woods, P., Ellingsen, K., Gauss, M., Isaksen, I., Blumenstock, T., Hase, F., Kramer, I., Camy-peyret, C., Chelin, P., Mahieu, E., Demoulin, P., Duchatelet, P., Mellqvist, J., Strandberg, A., Velazco, V., Notholt, J., Sussmann, R., Stremme, W., and Rockmann, A.: The exploitation of ground-based Fourier transform infrared observations for the evaluation of tropospheric trends of greenhouse gases over Europe, Environ. Sci. , 2, 283–293, 2005.

Derwent, R., Simmonds, P., Seuring, S., and Dimmer, C.: Observations and interpretation of the seasonal cycles in the surface concentrations of ozone and carbon monoxide at Mace Head, Ireland from 1990 to 1994, Atmos. Environ., 32, 145–157, 1998.

Dlugokencky, E. J., Bruhwiler, L., White, J. W. C., Emmons, L. K., Novelli, P. C., Montzka, S. A., Masarie, K. A., Lang, P. M., Crotwell, A. M., Miller, J. B., and Gatti, L. V.: Observational constraints on recent increases in the atmospheric CH4 burden, Geophys. Res. Lett., 36, L18803 doi:10.1029/2009gl039780, 2009.

Duchatelet, P., Demoulin, P., Hase, F., Ruhnke, R., Feng, W., Chipperfield, M. P., Bernath, P. F., Boone, C. D., Walker, K. A., and Mahieu, E.: Hydrogen fluoride total and partial column time series above the Jungfraujoch from long-term FTIR measurements: Impact of the line-shape model, characterization of the error budget and seasonal cycle, and comparison with satellite and model data, J. Geophys. Res.-Atmos., 115, D22306, doi:10.1029/2010jd014677, 2010.

EDGAR: European Commission, Joint Research Centre (JRC)/Netherlands Environmental Assessment Agency (PBL), Emission Database for Global Atmospheric Research (EDGAR), release version 4.0. http://edgar.jrc.ec.europa.eu, 2009.

Ehhalt, D. H., Schmidt, U., Zander, R., Demoulin, P., and Rinsland, C.: Seasonal cycle and secular trend of the total and tropospheric column abundance of ethane above the Jungfraujoch, J. Geophys. Res., 96, 4985–4994, 1991.

Emmons, L. K., Hauglustaine, D. A., Müller, J.-F., Carroll, M. A., Brasseur, G. P., Brunner, D., Staehelin, J., Thouret, V., and Marenco, A.: Data composites of airborne observations of tropospheric ozone and its precursors, J. Geophys. Res., 105, 20497-2-0538, 2000.

Fagerli, H., Legrand, M., Preunkert, S., Vestreng, V., Simpson, D., and Cerqueira, M.: Modeling historical long-term trends of sulfate, ammonium, and elemental carbon over Europe: A comparison with ice core records in the Alps, J. Geophys. Res.-Atmos., 112, D23s13 doi:10.1029/2006jd008044, 2007.

Fagerli, H. and Aas, W.: Trends of nitrogen in air and precipitation: Model results and observations at EMEP sites in Europe, 1980–2003, Environ. Pollut., 154, 448–461, doi:10.1016/j.envpol.2008.01.024, 2008.

Finlayson-Pitts, B. J. and Pitts, J. N.: Chemistry of the upper and lower atmosphere : theory, experiments, and applications, Academic Press, San Diego, xxii, 969 pp., 2000.

Fiore, A. M., Dentener, F. J., Wild, O., Cuvelier, C., Schultz, M. G., Hess, P., Textor, C., Schulz, M., Doherty, R. M., Horowitz, L. W., MacKenzie, I. A., Sanderson, M. G., Shindell, D. T., Stevenson, D. S., Szopa, S., Van Dingenen, R., Zeng, G., Atherton, C., Bergmann, D., Bey, I., Carmichael, G., Collins, W. J., Duncan, B. N., Faluvegi, G., Folberth, G., Gauss, M., Gong, S., Hauglustaine, D., Holloway, T., Isaksen, I. S. A., Jacob, D. J., Jonson, J. E., Kaminski, J. W., Keating, T. J., Lupu, A., Marmer, E., Montanaro, V., Park, R. J., Pitari, G., Pringle, K. J., Pyle, J. A., Schroeder, S., Vivanco, M. G., Wind, P., Wojcik, G., Wu, S., and Zuber, A.: Multimodel estimates of intercontinental source-receptor relationships for ozone pollution, J. GEOPHYS RES-ATMOS, 114, D04301 doi:10.1029/2008jd010816, 2009.

Gardiner, T., Forbes, A., de Mazire, M., Vigouroux, C., Mahieu, E., Demoulin, P., Velazco, V., Notholt, J., Blumenstock, T., Hase, F., Kramer, I., Sussmann, R., Stremme, W., Mellqvist, J., Strandberg, A., Ellingsen, K., and Gauss, M.: Trend analysis of greenhouse gases over Europe measured by a network of ground-based remote FTIR instruments, Atmos. Chem. Phys., 8, 6719–6727, doi:10.5194/acp-8-6719-2008, 2008.

Granier, C., Petron, G., Müller, J. F., and Brasseur, G.: The impact of natural and anthropogenic hydrocarbons on the tropospheric budget of carbon monoxide, Atmos. Environ., 34, 5255–5270, 2000.

Gilge, S., Plass-Duelmer, C., Fricke, W., Kaiser, A., Ries, L., Buchmann, B., and Steinbacher, M.: Ozone, carbon monoxide and nitrogen oxides time series at four alpine GAW mountain stations in central Europe, 2010.

Guenther, A. B., Zimmerman, P. R., Harley, P. C., Monson, R. K., and Fall, R.: Isoprene and Monoterpene Emission Rate Variability – Model Evaluations and Sensitivity Analyses, J. Geophys. Res.-Atmos., 98, 12609–12617, 1993.

Hansen, J., Sato, M., Ruedy, R., Lo, K., Lea, D. W., and Medina-Elizade, M.: Global temperature change, P Natl Acad Sci USA,

103, 14288–14293, doi:10.1073/pnas.0606291103, 2006.

Hase, F., Blumenstock, T., and Paton-Walsh, C.: Analysis of the instrumental line shape of high-resolution Fourier transform IR spectrometers with gas cell measurements and new retrieval software, Appl. Optics, 38, 3417–3422, 1999.

Hase, F., Hannigan, J. W., Coffey, M. T., Goldman, A., Hopfner, M., Jones, N. B., Rinsland, C. P., and Wood, S. W.: Intercomparison of retrieval codes used for the analysis of high-resolution, ground-based FTIR measurements, J. Quant. Spectrosc. Ra., 87, 25–52, doi:10.1016/j.jqsrt.2003.12.008, 2004.

Holloway, T., Levy, H., and Kasibhatla, P.: Global distribution of carbon monoxide, J. Geophys. Res.-Atmos., 105, 12123–12147, 2000.

HTAP, T.: Hemispheric Transport of air pollution 2007 Economic commision for Europe, Geneva, Air Pollution Studies No. 16, United Nations, New York and Geneva, 2007.

Isaksen, I. S. A., Granier, C., Myhre, G., Berntsen, T. K., Dalsoren, S. B., Gauss, M., Klimont, Z., Benestad, R., Bousquet, P., Collins, W., Cox, T., Eyring, V., Fowler, D., Fuzzi, S., Jockel, P., Laj, P., Lohmann, U., Maione, M., Monks, P., Prevot, A. S. H., Raes, F., Richter, A., Rognerud, B., Schulz, M., Shindell, D., Stevenson, D. S., Storelvmo, T., Wang, W. C., van Weele, M., Wild, M., and Wuebbles, D.: Atmospheric composition change: Climate-Chemistry interactions, Atmos. Environ., 43, 5138–5192, doi:10.1016/j.atmosenv.2009.08.003, 2009.

Jonson, J. E., Simpson, D., Fagerli, H., and Solberg, S.: Can we explain the trends in European ozone levels?, Atmos. Chem. Phys., 6, 51–66, doi:10.5194/acp-6-51-2006, 2006.

Jonson, J. E., Stohl, A., Fiore, A. M., Hess, P., Szopa, S., Wild, O., Zeng, G., Dentener, F. J., Lupu, A., Schultz, M. G., Duncan, B. N., Sudo, K., Wind, P., Schulz, M., Marmer, E., Cuvelier, C., Keating, T., Zuber, A., Valdebenito, A., Dorokhov, V., De Backer, H., Davies, J., Chen, G. H., Johnson, B., Tarasick, D. W., Stübi, R., Newchurch, M.J., von der Gathen, P., Steinbrecht, W., and Claude, H.: A multi-model analysis of vertical ozone profiles, Atmos. Chem. Phys., 10, 5759–5783, doi:10.5194/acp-10-5759-2010, 2010.

Khalil, M. A. K. and Rasmussen, R. A.: Carbon-Monoxide in the Earths Atmosphere – Indications of a Global Increase, Nature, 332, 242–245, 1988.

Khalil, M. A. K. and Rasmussen, R. A.: Global Decrease in Atmospheric Carbon-Monoxide Concentration, Nature, 370, 639–641, 1994.

Källén, E.: HIRLAM documentation manual. System 2.5. Technical report, HIRLAM, p. 178, p. 55, appendix, available from SMHI, S-60176 Norrköping, Sweden., 1996.

Lelieveld, J., Peters, W., Dentener, F. J., and Krol, M. C.: Stability of tropospheric hydroxyl chemistry, J. Geophys. Res.-Atmos., 107, 4715, doi:10.1029/2002jd002272, 2002.

Lenschow, H. S. and Tsyro, S.: Meteorological input data for EMEP/MSC-W air pollution models, EMEP MSC-W Note 2/2000, The Norwegian Meteorological Institute, Oslo, Norway, 2000.

Logan, J. A.: An analysis of ozonesonde data for the troposphere: Recommendations for testing 3-D models and development of a gridded climatology for tropospheric ozone, J. Geophys. Res.-Atmos., 104, 16115–16149, 1999.

Mahieu, E., Zander, R., Delbouille, L., Demoulin, P., Roland, G., and Servais, C.: Observed trends in total vertical column abundances of atmospheric gases from IR solar spectra recorded at the Jungfraujoch, J. Atmos. Chem., 28, 227–243, 1997.

Metzger, S., Dentener, F., Pandis, S., and Lelieveld, J.: Gas/aerosol partitioning: 1. A computationally efficient model, J. Geophys. Res.-Atmos., 107, 4312, doi:10.1029/2001jd001102, 2002.

Monks, P. S., Granier, C., Fuzzi, S., Stohl, A., Williams, M. L., Akimoto, H., Amann, M., Baklanov, A., Baltensperger, U., Bey, I., Blake, N., Blake, R. S., Carslaw, K., Cooper, O. R., Dentener, F., Fowler, D., Fragkou, E., Frost, G. J., Generoso, S., Ginoux, P., Grewe, V., Guenther, A., Hansson, H. C., Henne, S., Hjorth, J., Hofzumahaus, A., Huntrieser, H., Isaksen, I. S. A., Jenkin, M. E., Kaiser, J., Kanakidou, M., Klimont, Z., Kulmala, M., Laj, P., Lawrence, M. G., Lee, J. D., Liousse, C., Maione, M., McFiggans, G., Metzger, A., Mieville, A., Moussiopoulos, N., Orlando, J. J., O'Dowd, C. D., Palmer, P. I., Parrish, D. D., Petzold, A., Platt, U., Poschl, U., Prevot, A. S. H., Reeves, C. E., Reimann, S., Rudich, Y., Sellegri, K., Steinbrecher, R., Simpson, D., ten Brink, H., Theloke, J., van der Werf, G. R., Vautard, R., Vestreng, V., Vlachokostas, C., and von Glasow, R.: Atmospheric composition change – global and regional air quality, Atmos. Environ., 43, 5268–5350, doi:10.1016/j.atmosenv.2009.08.021, 2009.

Montgomery, D. C., Jennings, C. L., and Kulahci, M.: Introduction to time series analysis and forecasting, Wiley series in probability and statistics, Wiley-Interscience, Hoboken, N. J., xi, 445 pp., 2008.

Montzka, S. A., Krol, M., Dlugokencky, E., Hall, B., Jockel, P., and Lelieveld, J.: Small Interannual Variability of Global Atmospheric Hydroxyl, Science, 331, doi:10.1126/science.1197640, 2011.

Novelli, P. C., Masarie, K. A., Lang, P. M., Hall, B. D., Myers, R. C., and Elkins, J. W.: Reanalysis of tropospheric CO trends: Effects of the 1997-1998 wildfires, J. Geophys. Res.-Atmos., 108, 4464, doi:10.1029/2002jd003031, 2003.

Passant, N. R.: Speciation of UK emissions of non-methane volatile organic compounds, AEAT/ENV/R/0545 Issue 1, 2002.

Reidmiller, D. R., Fiore, A. M., Jaffe, D. A., Bergmann, D., Cuvelier, C., Dentener, F. J., Duncan, B. N., Folberth, G., Gauss, M., Gong, S., Hess, P., Jonson, J. E., Keating, T., Lupu, A., Marmer, E., Park, R., Schultz, M. G., Shindell, D. T., Szopa, S., Vivanco, M. G., Wild, O., and Zuber, A.: The influence of foreign vs. North American emissions on surface ozone in the US, Atmos. Chem. Phys., 9, 5027–5042, doi:10.5194/acp-9-5027-2009, 2009.

Rinsland, C. P., Jones, N. B., Connor, B. J., Logan, J. A., Pougatchev, N. S., Goldman, A., Murcray, F. J., Stephen, T. M., Pine, A. S., Zander, R., Mahieu, E., and Demoulin, P.: Northern and southern hemisphere ground-based infrared spectroscopic measurements of tropospheric carbon monoxide and ethane, J. Geophys. Res.-Atmos., 103, 28197–28217, 1998.

Rinsland, C. P., Mahieu, E., Zander, R., Demoulin, P., Forrer, J., and Buchmann, B.: Free tropospheric CO, C_2H_6, and HCN above central Europe: Recent measurements from the Jungfraujoch station including the detection of elevated columns during 1998, J. Geophys. Res.-Atmos., 105, 24235–24249, 2000.

Rinsland, C. P., Goldman, A., Hannigan, J. W., Wood, S. W., Chiou, L. S., and Mahieu, E.: Long-term trends of tropospheric carbon monoxide and hydrogen cyanide from analysis of high resolution infrared solar spectra, J. Quant. Spectrosc. Ra., 104, 40–51, doi:10.1016/j.jqsrt.2006.08.008, 2007.

Rodgers, C. D.: Inverse Methods for Atmospheric Sounding, Series on Atmospheric, Oceanic and Planetary Physics, 2, 55–63, 2000.

Rothman, L. S., Jacquemart, D., Barbe, A., Benner, D. C., Birk, M., Brown, L. R., Carleer, M. R., Chackerian, C., Chance, K., Coudert, L. H., V, D., Devi, V. M., Flaud, J. M., Gamache, R. R., Goldman, A., Hartmann, J. M., Jucks, K. W., Maki, A. G., Mandin, J. Y., Massie, S. T., Orphal, J., Perrin, A., Rinsland, C. P., Smith, M. A. H., Tennyson, J., Tolchenov, R. N., Toth, R. A., Vander Auwera, J., Varanasi, P., and Wagner, G.: The HITRAN 2004 molecular spectroscopic database, J. Quant. Spectrosc. Ra., 96, 139–204, doi:10.1016/j.jqsrt.2004.10.008, 2005.

Sanderson, M. G., Dentener, F. J., Fiore, A. M., Cuvelier, C., Keating, T. J., Zuber, A., Atherton, C. S., Bergmann, D. J., Diehl, T., Doherty, R. M., Duncan, B. N., Hess, P., Horowitz, L. W., Jacob, D. J., Jonson, J. E., Kaminski, J. W., Lupu, A., MacKenzie, I. A., Mancini, E., Marmer, E., Park, R., Pitari, G., Prather, M. J., Pringle, K. J., Schroeder, S., Schultz, M. G., Shindell, D. T., Szopa, S., Wild, O., and Wind, P.: A multi-model study of the hemispheric transport and deposition of oxidised nitrogen, Geophys. Res. Lett., 35, L17815, doi:10.1029/2008gl035389, 2008.

Shindell, D. T., Faluvegi, G., Stevenson, D. S., Krol, M. C., Emmons, L. K., Lamarque, J. F., Petron, G., Dentener, F. J., Ellingsen, K., Schultz, M. G., Wild, O., Amann, M., Atherton, C. S., Bergmann, D. J., Bey, I., Butler, T., Cofala, J., Collins, W. J., Derwent, R. G., Doherty, R. M., Drevet, J., Eskes, H. J., Fiore, A. M., Gauss, M., Hauglustaine, D. A., Horowitz, L. W., Isaksen, I. S. A., Lawrence, M. G., Montanaro, V., Muller, J. F., Pitari, G., Prather, M. J., Pyle, J. A., Rast, S., Rodriguez, J. M., Sanderson, M. G., Savage, N. H., Strahan, S. E., Sudo, K., Szopa, S., Unger, N., van Noije, T. P. C., and Zeng, G.: Multimodel simulations of carbon monoxide: Comparison with observations and projected near-future changes, J. Geophys. Res.-Atmos., 111, D19306, doi:10.1029/2006jd007100, 2006.

Shindell, D. T., Chin, M., Dentener, F., Doherty, R. M., Faluvegi, G., Fiore, A. M., Hess, P., Koch, D. M., MacKenzie, I. A., Sanderson, M. G., Schultz, M. G., Schulz, M., Stevenson, D. S., Teich, H., Textor, C., Wild, O., Bergmann, D. J., Bey, I., Bian, H., Cuvelier, C., Duncan, B. N., Folberth, G., Horowitz, L. W., Jonson, J., Kaminski, J. W., Marmer, E., Park, R., Pringle, K. J., Schroeder, S., Szopa, S., Takemura, T., Zeng, G., Keating, T. J., and Zuber, A.: A multi-model assessment of pollution transport to the Arctic, Atmos. Chem. Phys., 8, 5353–5372, doi:10.5194/acp-8-5353-2008, 2008.

Simpson, D., Guenther, A., Hewitt, C. N., and Steinbrecher, R.: Biogenic Emissions in Europe .1. Estimates and Uncertainties, J. Geophys. Res.-Atmos., 100, 22875–22890, 1995.

Simpson, D., Winiwarter, W., Borjesson, G., Cinderby, S., Ferreiro, A., Guenther, A., Hewitt, C. N., Janson, R., Khalil, M. A. K., Owen, S., Pierce, T. E., Puxbaum, H., Shearer, M., Skiba, U., Steinbrecher, R., Tarrason, L., and Oquist, M. G.: Inventorying emissions from nature in Europe, J. Geophys. Res.-Atmos., 104, 8113–8152, 1999.

Simpson, D., Fagerli, H., Jonson, J., Tsyro, S., Wind, P., and Tuovinen, J.-P.: The EMEP Unified Eulerian Model. Model Description The Norwegian Meteorological Institute, Oslo, Norway, 2003a.

Simpson, D., Fagerli, H., Solberg, S., and Aas, W.: Photo-oxidants, EMEP MSC-W Report 1/2003, Part II, Unified EMEP Model performance, Norwegian Meteorological Institute, Oslo, Norway, 1/2003, Part II, 2003b.

Simpson, D., Tuovinen, J. P., Emberson, L., and Ashmore, M. R.: Characteristics of an ozone deposition module II: Sensitivity analysis, Water Air Soil. Poll., 143, 123–137, 2003c.

Simpson, D., Fagerli, H., Hellsten, S., Knulst, J. C., and Westling, O.: Comparison of modelled and monitored deposition fluxes of sulphur and nitrogen to ICP-forest sites in Europe, Biogeosciences, 3, 337–355, 2006, http://www.biogeosciences.net/3/337/2006/.

Simpson, D., Michael Gauss, S. T., and Valdebenito, A.: Model Updates Transboundary acidification, eutrophication and ground level ozone in Europe EMEP Status Report 1/2010, The Norwegian Meteorological Institute, Oslo, Norway, 2010.

Stevenson, D. S., Dentener, F. J., Schultz, M. G., Ellingsen, K., van Noije, T. P. C., Wild, O., Zeng, G., Amann, M., Atherton, C. S., Bell, N., Bergmann, D. J., Bey, I., Butler, T., Cofala, J., Collins, W. J., Derwent, R. G., Doherty, R. M., Drevet, J., Eskes, H. J., Fiore, A. M., Gauss, M., Hauglustaine, D. A., Horowitz, L. W., Isaksen, I. S. A., Krol, M. C., Lamarque, J. F., Lawrence, M. G., Montanaro, V., Muller, J. F., Pitari, G., Prather, M. J., Pyle, J. A., Rast, S., Rodriguez, J. M., Sanderson, M. G., Savage, N. H., Shindell, D. T., Strahan, S. E., Sudo, K., and Szopa, S.: Multimodel ensemble simulations of present-day and near-future tropospheric ozone, J. Geophys. Res.-Atmos., 111, D08301, doi:10.1029/2005jd006338, 2006.

Tarrason, L., Fagerli, H., Gauss, M., Ny'ıri, A., Simpson, D., Tsyro, S., and Aas, W.: S, N and O3 in EEECA countries, in: In Transboundary Acidification, Eutrophication and Ground Level Ozone in Europe in 2006. EMEP Status Report 1/2008, 67–86, The Norwegian Meteorological Institute, Oslo, Norway, 2008.

van der Werf, G. R., Randerson, J. T., Giglio, L., Collatz, G. J., Kasibhatla, P. S., and Arellano Jr., A. F.: Interannual variability in global biomass burning emissions from 1997 to 2004, Atmos. Chem. Phys., 6, 3423–3441, doi:10.5194/acp-6-3423-2006, 2006.

Warneck, P.: Chemistry of the natural atmosphere, 2nd ed., This is volume 71 in the International geophysics series, Academic Press, San Diego, xvii, 927 pp., 2000.

Warneke, C., de Gouw, J. A., Del Negro, L., Brioude, J., McKeen, S., Stark, H., Kuster, W. C., Goldan, P. D., Trainer, M., Fehsenfeld, F. C., Wiedinmyer, C., Guenther, A. B., Hansel, A., Wisthaler, A., Atlas, E., Holloway, J. S., Ryerson, T. B., Peischl, J., Huey, L. G., and Hanks, A. T. C.: Biogenic emission measurement and inventories determination of biogenic emissions in the eastern United States and Texas and comparison with biogenic emission inventories, J. Geophys. Res.-Atmos., 115, D00F18, doi:10.1029/2009JD012445, 2010.

Vieno, M., Dore, A. J., Stevenson, D. S., Doherty, R., Heal, M. R., Reis, S., Hallsworth, S., Tarrason, L., Wind, P., Fowler, D., Simpson, D., and Sutton, M. A.: Modelling surface ozone during the 2003 heat-wave in the UK, Atmos. Chem. Phys., 10, 7963–7978, doi:10.5194/acp-10-7963-2010, 2010.

Vigouroux, C., De Mazire, M., Demoulin, P., Servais, C., Hase, F., Blumenstock, T., Kramer, I., Schneider, M., Mellqvist, J., Strandberg, A., Velazco, V., Notholt, J., Sussmann, R., Stremme, W., Rockmann, A., Gardiner, T., Coleman, M., and Woods, P.: Evaluation of tropospheric and stratospheric ozone trends over Western Europe from ground-based FTIR network observations, Atmos. Chem. Phys., 8, 6865–6886, doi:10.5194/acp-8-6865-

2008, 2008.

Xiao, Y. P., Logan, J. A., Jacob, D. J., Hudman, R. C., Yantosca, R., and Blake, D. R.: Global budget of ethane and regional constraints on US sources, J. Geophys. Res.-Atmos., 113, D21306, doi:10.1029/2007jd009415, 2008.

Yurganov, L. N., Blumenstock, T., Grechko, E. I., Hase, F., Hyer, E. J., Kasischke, E. S., Koike, M., Kondo, Y., Kramer, I., Leung, F. Y., Mahieu, E., Mellqvist, J., Notholt, J., Novelli, P. C., Rinsland, C. P., Scheel, H. E., Schulz, A., Strandberg, A., Sussmann, R., Tanimoto, H., Velazco, V., Zander, R., and Zhao, Y.: A quantitative assessment of the 1998 carbon monoxide emission anomaly in the Northern Hemisphere based on total column and surface concentration measurements, J. Geophys. Res.-Atmos., 109, D15305, doi:10.1029/2004jd004559, 2004.

Yurganov, L. N., Duchatelet, P., Dzhola, A. V., Edwards, D. P., Hase, F., Kramer, I., Mahieu, E., Mellqvist, J., Notholt, J., Novelli, P. C., Rockmann, A., Scheel, H. E., Schneider, M., Schulz, A., Strandberg, A., Sussmann, R., Tanimoto, H., Velazco, V., Drummond, J. R., and Gille, J. C.: Increased Northern Hemispheric carbon monoxide burden in the troposphere in 2002 and 2003 detected from the ground and from space, Atmos. Chem. Phys., 5, 563–573, doi:10.5194/acp-5-563-2005, 2005.

Zhao, Y., Strong, K., Kondo, Y., Koike, M., Matsumi, Y., Irie, H., Rinsland, C. P., Jones, N. B., Suzuki, K., Nakajima, H., Nakane, H., and Murata, I.: Spectroscopic measurements of tropospheric CO, C2H6, C2H2,and HCN in northern Japan, J. Geophys. Res.-Atmos., 107, 4343, doi:10.1029/2001jd000748, 2002.